Hepatocellular carcinoma originates from hepatocytes and not from the progenitor/biliary compartment

Xueru Mu,[1,2] Regina Español-Suñer,[3] Ingmar Mederacke,[1] Silvia Affò,[1] Rita Manco,[3] Christine Sempoux,[4] Frédéric P. Lemaigre,[5] Arlind Adili,[6] Detian Yuan,[6] Achim Weber,[7] Kristian Unger,[8] Mathias Heikenwälder,[6] Isabelle A. Leclercq,[3] and Robert F. Schwabe[1]

[1]Department of Medicine, Columbia University, New York, New York, USA. [2]Institute of Oncology, Provincial Hospital Affiliated with Shandong University, Shandong University, Jinan, China. [3]Laboratory of Hepato-Gastroenterology, Institut de Recherche Expérimentale et Clinique, Université catholique de Louvain, Brussels, Belgium. [4]Department of Pathology, St. Luc University Hospital and Université catholique de Louvain, Brussels, Belgium. [5]Liver and Pancreas Development Unit, de Duve Institute, Université catholique de Louvain, Brussels, Belgium. [6]Institute of Virology, Technische Universität München/Helmholtz Zentrum München, Munich, Germany. [7]Institute of Surgical Pathology, University Hospital Zurich, Zurich, Switzerland. [8]Research Unit of Radiation Cytogenetics, Helmholtz Zentrum München, German Research Center for Environmental Health, Neuherberg, Germany.

In many organs, including the intestine and skin, cancers originate from cells of the stem or progenitor compartment. Despite its nomenclature, the cellular origin of hepatocellular carcinoma (HCC) remains elusive. In contrast to most organs, the liver lacks a defined stem cell population for organ maintenance. Previous studies suggest that both hepatocytes and facultative progenitor cells within the biliary compartment are capable of generating HCC. As HCCs with a progenitor signature carry a worse prognosis, understanding the origin of HCC is of clinical relevance. Here, we used complementary fate-tracing approaches to label the progenitor/biliary compartment and hepatocytes in murine hepatocarcinogenesis. In genotoxic and genetic models, HCCs arose exclusively from hepatocytes but never from the progenitor/biliary compartment. Cytokeratin 19–, A6- and α-fetoprotein–positive cells within tumors were hepatocyte derived. In summary, hepatocytes represent the cell of origin for HCC in mice, and a progenitor signature does not reflect progenitor origin, but dedifferentiation of hepatocyte-derived tumor cells.

Introduction

Hepatocellular carcinoma (HCC) is the third leading cause of cancer mortality worldwide, with approximately 700,000 new cases diagnosed every year (1, 2). HCC typically develops in patients with chronic liver disease. Among these, viral hepatitis, nonalcoholic fatty liver disease, and alcoholic liver disease are the leading causes of HCC (2). Chronic liver injury, triggering permanent hepatocellular damage, hepatocyte regeneration, and inflammation, is thought to be the unifying principle that promotes carcinogenesis in these pathophysiologically distinct diseases. In the developing liver, bipotent hepatoblasts differentiate into hepatocytes and cholangiocytes and function as a main cellular source for both lineages (3). However, in the adult liver, cell turnover is minimal, and bipotent progenitors are typically absent (3). In contrast to many organs that have a hierarchical organization depending on well-defined stem cell populations, such as intestine and skin (4–6), the fully differentiated hepatocyte is endowed with an almost infinite capacity to regenerate (7). Accordingly, regeneration following most types of injury or after partial hepatectomy is achieved from the hepatocyte pool without major contribution of progenitor cells (3, 8). However, when liver injury is chronic and when the ability of mature hepatocytes to proliferate is blocked, a reserve cell compartment located within the biliary compartment — often termed oval cells or liver progenitor cells (LPCs) — expands in patients and in experimental injury models and may contribute to the formation of hepatocytes (3, 7, 9–13). However, several recent fate-tracing studies have challenged a major role for the LPC/biliary compartment in the formation of hepatocytes, showing either no or only very little contribution to the hepatocyte pool (8, 14–18). On the other hand, the LPC/biliary compartment is capable of generating functional hepatocytes in zebrafish (19), indicating that its contribution may be model-, disease-, or species-specific. Moreover, recent studies have suggested that hepatic stellate cells (HSCs) may function as multipotent progenitor cells that generate functional hepatocytes and cholangiocytes (20). Thus, 3 potential cellular sources — hepatocytes, the LPC/biliary compartment and HSCs — may, in theory, function as progenitor cells and the cellular source for newly generated hepatocytes.

In view of the key roles of stem and progenitor cells in the maintenance of many tissues, it is not surprising that these are also the cells of origin in cancer of the intestine (21, 22), skin (23, 24), and hematopoietic system (25). In contrast, the cellular origin of HCC remains elusive, with the above-discussed contributors to homeostasis and regeneration of the adult liver, namely hepatocytes, the LPC/biliary compartment, and HSCs, representing potential sources. Of note, the expansion of LPCs has consistently been noted after treatment with hepatic carcinogens (26, 27), which has led to the suggestion that HCC may be derived from the LPC/biliary compartment (26, 28, 29). Moreover, the expression of progenitor markers and accumulation of LPCs are commonly observed in rodent models as well as in human HCC (30, 31). Therefore, the reemergence of LPCs in the chronically injured

Authorship note: Xueru Mu and Regina Español-Suñer contributed equally to this work.
Conflict of interest: The authors have declared that no conflict of interest exists.
Submitted: July 17, 2014; **Accepted:** July 23, 2015.
Reference information: *J Clin Invest*. 2015;125(10):3891–3903. doi:10.1172/JCI77995.

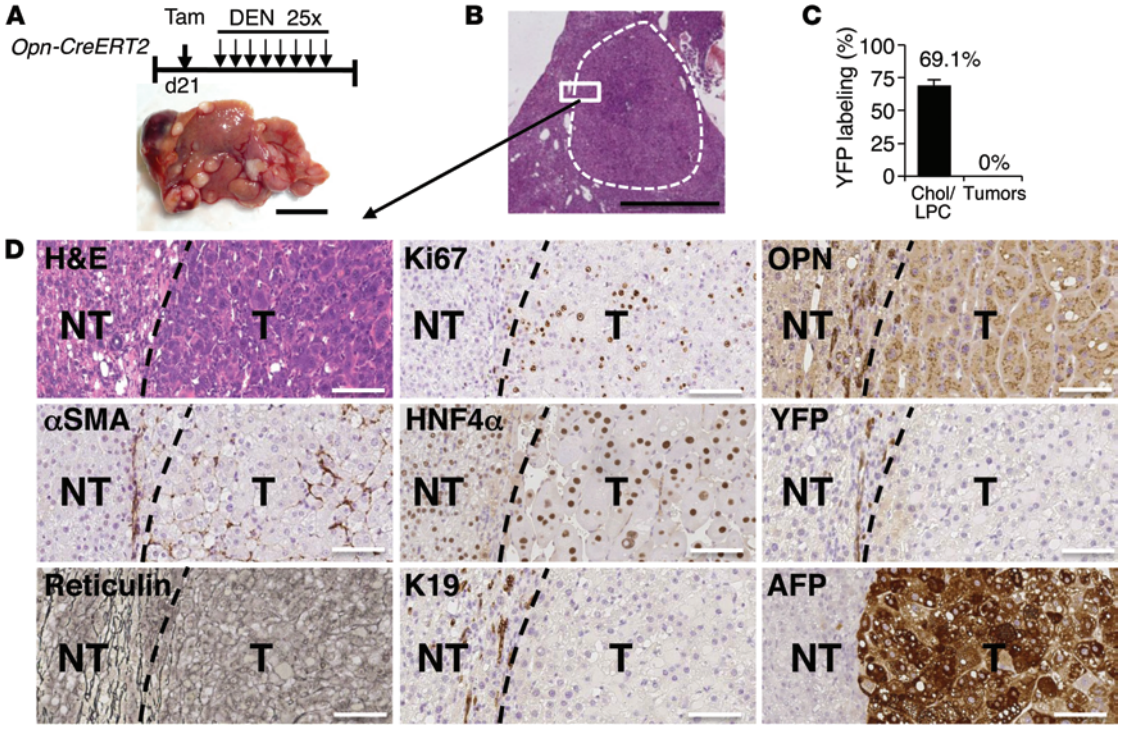

Figure 1. HCC does not derive from the LPC/biliary compartment. Tamoxifen-treated *Opn-CreERT2* mice expressing the YFP Cre reporter were subjected to 25 injections of DEN (n = 33). (**A** and **B**) Mice developed macroscopically (**A**) and microscopically (**B**) visible HCCs. Tam, tamoxifen. (**C** and **D**) While the K19-positive biliary/LPC compartment was tagged efficiently by YFP, no HCCs were YFP positive. HCCs were delineated by an α-SMA–positive border and infiltrated by myofibroblasts; HCCs displayed a disrupted reticulin meshwork, high Ki67 expression levels, focally expressed OPN and AFP, and were surrounded by a patchy K19-positive and YFP-positive DR. Scale bars: 1 cm (**A** and **B**); 100 μm (**D**). Chol, cholangiocyte; NT, nontumor; T, tumor.

liver may link regeneration to hepatocarcinogenesis. As HCC with a progenitor signature is clinically more aggressive, it has been suggested that the progenitor origin of HCC determines tumor biology and negatively affects outcome (31). Importantly, both LPCs and hepatocytes have the capacity to generate tumors in vivo when transduced with H-RAS and SV40LT (32). However, the relative contribution of these 2 cell types to cancer formation in the context of chronic hepatocellular injury in vivo remains unknown. The high degree of plasticity in the liver is further highlighted by recent studies showing that cholangiocarcinoma can be derived not only from cholangiocytes (33) but also from hepatocytes (34, 35). Given these findings in cholangiocarcinoma, it is conceivable that there are also multiple cellular sources for HCC. Using complementary strategies to label the LPC/biliary compartment, hepatocytes, and HSCs, we demonstrate that hepatocytes, but neither the LPC/biliary compartment nor HSCs, function as a cellular source for HCC. Moreover, LPCs found in HCC were derived from hepatocytes, suggesting that hepatocyte-derived HCC may dedifferentiate into an LPC-like immature phenotype.

Results

HCC does not originate from the LPC/biliary compartment. To test the hypothesis that HCC is derived from the LPC/biliary compartment, we used tamoxifen-inducible osteopontin-i*CreER*^{T2} (*Opn*-i*CreER*^{T2}) *Rosa26R*^{YFP} mice (referred to herein as *Opn-CreERT2* mice) to label progenitor and biliary cells. Tamoxifen injection in the postnatal period leads to recombination of the *Rosa26R*^{YFP} locus and to permanent expression of yellow fluorescent protein (YFP) in OPN-expressing cells. As reported elsewhere (15), upon tamoxifen injection, YFP expression is restricted to the LPC/biliary compartment and does not occur in hepatocytes, stellate cells, or Kupffer cells (Supplemental Figure 1; supplemental material available online with this article; doi:10.1172/JCI77995DS1). Using this system, between 69% and 84% of the LPC/biliary compartment and its progeny were permanently tagged with YFP in this study (Figure 1C, Figure 2D, and Supplemental Figure 1A), and thus, development of YFP$^+$ HCC would indicate a progenitor/biliary origin.

First, HCCs were induced by chronic administration of diethylnitrosamine (DEN), resulting in HCC development in the setting of chronic injury, inflammation, and fibrosis (36). Tamoxifen was injected on postpartum (pp) day 21 (n = 44), followed after a 4-week washout period by repeated administration of DEN. At the time of sacrifice, macroscopic tumors were observed in all livers (Figure 1A and Table 1). These tumors were well delineated and exhibited enlargement of hepatocytic plates, a high proliferative index, disruption of the reticulin network, absence of portal tracts, and focal expression of α-fetoprotein (AFP) and OPN (Figure 1, B–D). Altogether, 250 tumors were histologically evaluated by an experimental pathologist (C. Sempoux) and diagnosed as HCC. YFP immunostaining was performed to determine the cellular source of HCC. In all 250 tumors, YFP expression was missing (Table 1) and only seen in CK-19–positive and OPN-positive bile duct cells and in the ductular reaction (DR) that surrounds the tumors (Fig-

Table 1. Tracing of the LPC/biliary compartment in HCC models

Mouse	HCC induction	Liver analyzed (*n*)	Livers with HCCs (%)	No. of HCCs analyzed per liver (min–max)	Total no. of HCCs analyzed	% of HCCs traced as having LPC origin	% of K19$^+$ HCCs (no. of pos. HCCs/ no. of analyzed tumors)	% of A6$^+$ HCCs (no. of pos. HCCs/ no. of analyzed tumors)
Opn-CreERT2	TAM d 21 / DEN 25×	33	100%	1 to >25	>250	0	2% (5/250 analyzed)	14.7% (17/115 analyzed)
Opn-CreERT2	DEN d 15/TAM d 21–22	25	68%	1–20	>150	0	0% (0/150 analyzed)	Not det.
Opn-CreERT2	DEN d 15/TAM d 9–10	16	50%	420	>90	0	0% (0/90 analyzed)	26% (13/50 analyzed)
Opn-CreERT2	TAM d 9–10/DEN d 15/ CCl_4 20×	6	100%	1–15	30	0	0% (0/30 analyzed)	66.6% (20/30 analyzed)
Opn-CreERT2	CDE diet >1 yr	9	30%	1–2	4	0	0	Not det.
K19-CreERT	TAM d 10, DEN+CCl_4	5	100%	25–69	219	0	11.5% (15/131 analyzed)	35.1% (46/131 analyzed)
Pten$^{fl/fl}$ - K19-CreERT	*Pten* deletions in LPCs (TAM d 21)	4	0%	NA	NA	NA	NA	NA

20×, 20 injections; 25×, 25 injections; NA, not applicable; Not det., not determined; min, minimum; max, maximum; pos., positive.

ure 1, C and D). In a second model, HCCs were induced by a single DEN injection into 15-day-old (day 15) *Opn-CreERT2* mice. Tamoxifen was injected before (pp days 9–10; $n = 16$) or after (pp days 21–22; $n = 25$) DEN administration. The efficiency and specificity of the lineage tracing was equivalent (≈70%) and independent of the time of tamoxifen administration, and macroscopic tumors developed (Supplemental Figure 2, A and B) in 50% and 70% of the mice within 18 and 9 months, respectively (Table 1), consistent with the notion that tamoxifen treatment, in particular when given immediately before tumor induction, delays or inhibits tumor development (37). Two-hundred forty tumors induced by this method were diagnosed as HCC. YFP expression was absent in all HCCs (Table 1), while bile ducts and the DR found surrounding the tumors were YFP positive (Supplemental Figure 2, C and D). These findings were further confirmed in *Opn-CreERT2* mice treated with the combination of DEN and CCl_4, which mimics hepatocarcinogenesis in the setting of liver fibrosis (38). In this model, HCCs also displayed characteristic features such as loss of collagen IV staining, high proliferation, and expression of the progenitor/hepatoblast genes *Afp*, *Prom1*, and *H19* (Figure 2, A, B, and E). Again, none of the tumors were labeled with YFP, whereas bile ducts in nontumor liver were YFP positive (Figure 2, C and D, and Table 1). In a second model of LPC/biliary compartment labeling, achieved by the combination of tamoxifen-inducible *K19-CreERT* (39) and the Cre reporter mTom-mGFP, none of the arising DEN plus CCl_4–induced (DEN+CCl_4-induced) HCCs (0 of 219 tumors) were mGFP positive, i.e., derived from the *K19-CreERT*–labeled LPC/biliary compartment (Figure 2, F–I, Supplemental Figure 3, A–C, and Table 1). In summary, the absence of LPC/biliary compartment–labeled tumors confirms that in multiple genotoxic DEN-induced hepatocarcinogenesis models and in different Cre-Tg mice, HCCs do not arise from LPCs or biliary cells.

Genotoxic HCC originates from hepatocytes. As we found no evidence for the LPC/biliary compartment serving as the cellular source of HCC, we next investigated the alternative hypothesis that hepatocytes constitute the cellular source for HCC. To selectively label and trace hepatocytes during hepatocarcinogenesis, we used an adeno-associated virus serotype 8 (AAV8) expressing Cre recombinase under the control of the hepatocyte-specific thyroxin-binding globulin (TBG) promoter (AAV8-*Tbg-Cre*) in combination with *Rosa26$^{loxP\text{-}mTom\text{-}stop\text{-}loxP\text{-}mGFP}$* (mTom-mGFP) or *Rosa26$^{loxP\text{-}stop\text{-}loxP\text{-}ZsGreen1}$* (ZsGreen) Cre reporter mice. In ZsGreen Cre reporter mice, this approach labeled more than 96% of hepatocytes, without labeling any other hepatic compartment including F4/80-positive Kupffer cells, the cytokeratin-positive biliary and LPC compartments, desmin-positive HSCs, or endomucin-positive endothelial cells, as determined by IHC and confocal imaging (Supplemental Figure 4, A and C–G). This analysis was further confirmed by quantitative PCR (qPCR) of FACS-sorted cells that expressed the green fluorescent Cre reporter ZsGreen and showed at least the same level of *Alb* and *Ttr* expression as did primary hepatocytes, but virtually no expression of cholangiocyte markers *Krt7* and *Krt19*, HSC markers *Des* and *Lrat*, endothelial cell markers *Pecam* (CD31) and *Vwf*, or macrophage markers *Emr1* (F4/80) and *Cd68* (Supplemental Figure 4B). Together, these data confirm an efficient and highly specific labeling of hepatocytes by AAV8-*Tbg-Cre*, similar to what was observed in previous studies (40, 41). Following AAV8-*Tbg-Cre* infection on pp day 12, we used either the single agent DEN (data not shown) or the combination of DEN+CCl_4 to trigger hepatocarcinogenesis. These well-established protocols resulted in the development of well-delineated tumors in 100% of mice (Figure 3A). Although the average hepatocyte-labeling rate in the mTom-mGFP reporter mice was slightly below 96%, we observed, macroscopically and microscopically, an average rate of 99.7% of mGFP-positive tumors (average of $n = 10$ mice, 185 of 186 mGFP-positive tumors), i.e., hepatocyte-derived tumors, in DEN+CCl_4-treated mice (Figure 3, A–D, and Table 2). Because hepatocyte labeling did not reach 100%, and because we never observed any tumor arising from the LPC/biliary compartment by our complementary LPC/biliary compartment–labeling approaches, we consider it most likely that the single GFP-negative tumor arose from unlabeled hepatocytes rather than from the LPC/biliary compartment. Although tumors were macroscopically entirely green, microscopic analysis revealed the presence of unrecombined, nonhepatocyte-derived Tomato-positive cells. These tomato-positive cells consisted predominantly of CD31-positive endothelial cells and F4/80-positive macrophages (Supplemental Figure 5). Tumors were clearly defined as HCCs by pathological examination, which showed loss of the normal hepatic reticulin and collagen IV staining pattern, increased expression

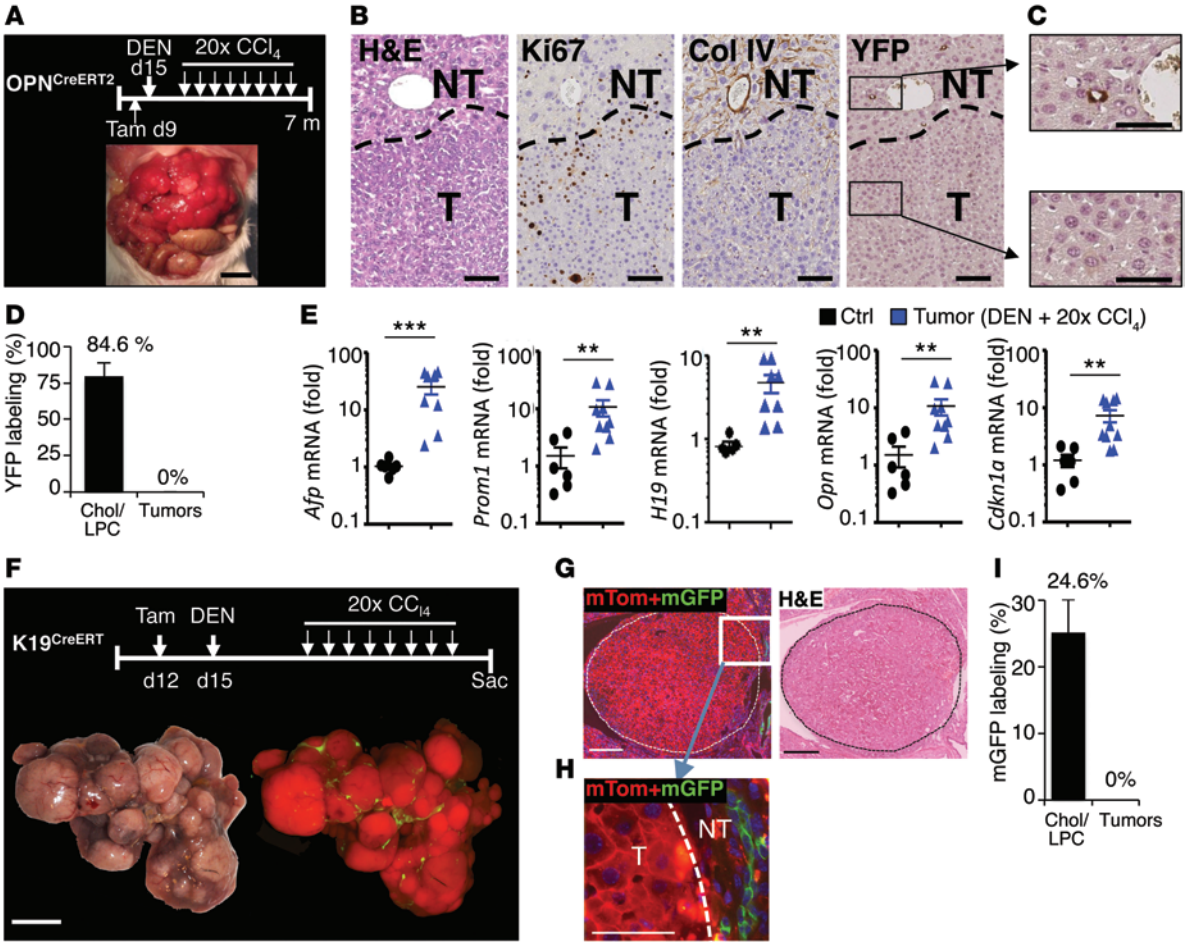

Figure 2. HCC does not derive from the LPC/biliary compartment in the DEN+CCl_4 model. Tamoxifen-treated *Opn-CreERT2* mice were treated with DEN followed by 20 injections (20×) of CCl_4 (n = 6). (**A** and **B**) Representative macroscopic (**A**) and histological images (**B**) showing typical HCC features such as high Ki67 expression levels and disruption of the collagen IV meshwork. Col IV, collagen IV. (**C** and **D**) The cholangiocyte/LPC compartment was YFP positive, but no HCCs were YFP positive (n = 6). (**E**) HCC and progenitor/hepatoblast markers determined by qPCR. (**F**–**I**) mTom-mGFP Cre reporter mice (n = 5) were treated with tamoxifen, followed by administration of DEN and 20 injections of CCl_4 for HCC induction. Representative images and fluorescent images of livers (**F**) and H&E- and GFP-stained liver sections at low (**G**) and high (**H**) magnification, demonstrating mGFP-positive ducts in nontumor areas but not in tumor areas. Quantification of GFP-labeled K19-positive cholangiocytes and tumors (n = 5) (**I**). Sac, sacrifice. Scale bars: 1 cm (**A** and **F**); 100 μm (**B** and **G**); 50 μm (**C** and **H**). $^{**}P < 0.01$, $^{***}P < 0.001$ by Mann-Whitney U test.

of the proliferation marker Ki67, an altered expression pattern of Gp73, loss of β-catenin, and upregulation of glutamine synthetase (Figure 3E). Histological analysis revealed a wide range of growth patterns including trabecular, steatotic, and solid and cytoplasmatic inclusions (Supplemental Figure 6A). Accordingly, tumors were diverse when analyzed by array comparative genomic hybridization (aCGH), which demonstrated chromosomal aberrations in each investigated mouse, with a wide range of genomic alterations rather than a specific pattern (Supplemental Figure 6B). Of note, comparison of genomic alteration in DEN+CCl_4-induced HCCs with a well-characterized set of human cryptogenic HCCs (42) revealed gains and losses of loci in various chromosomal regions congruent with genomic alterations in human HCC (Supplemental Figure 6C), further confirming the relevance of the model used here. Moreover, tumors expressed high mRNA levels of genes that are typically elevated in HCC, including *Gpc3*, *Golm1*, *mKi67*, *Tff3*, and *Tspan8* mRNA (Figure 3F). Importantly, every single DEN+CCl_4-induced tumor we examined showed at least 1 order of magnitude higher expression of the progenitor and hepatoblast markers *Afp* and *H19*, and almost all also contained much higher levels of *Prom1* (Figure 3G). These data clearly exclude the possibility that hepatocyte origin in the DEN+CCl_4 model is due to the lack of a progenitor signature in these tumors. To additionally address the possibility that LPC origin may only be revealed in models in which HCC arises in the setting of higher progenitor cell presence and turnover, we used the combination of DEN with either a choline-deficient, 0.15% ethionine-supplemented (CDE) diet or a 0.1% 3,5-diethoxycarbonyl-1,4-dihydro-collidin–supplemented (DDC-supplemented) diet (14, 15). Although the labeling of hepatocytes was less efficient in these experiments than in the above DEN+CCl_4 experiments, 98.3% of DEN+CDE diet–induced tumors and 95.6% of DEN+DDC diet–induced tumors were macroscopically and microscopically GFP positive (Supplemental Figure 7, A–D). When only mice with at least 90% hepatocyte labeling were included in the analysis, 100% of tumors were GFP positive (data not shown), again suggesting that the few GFP-negative

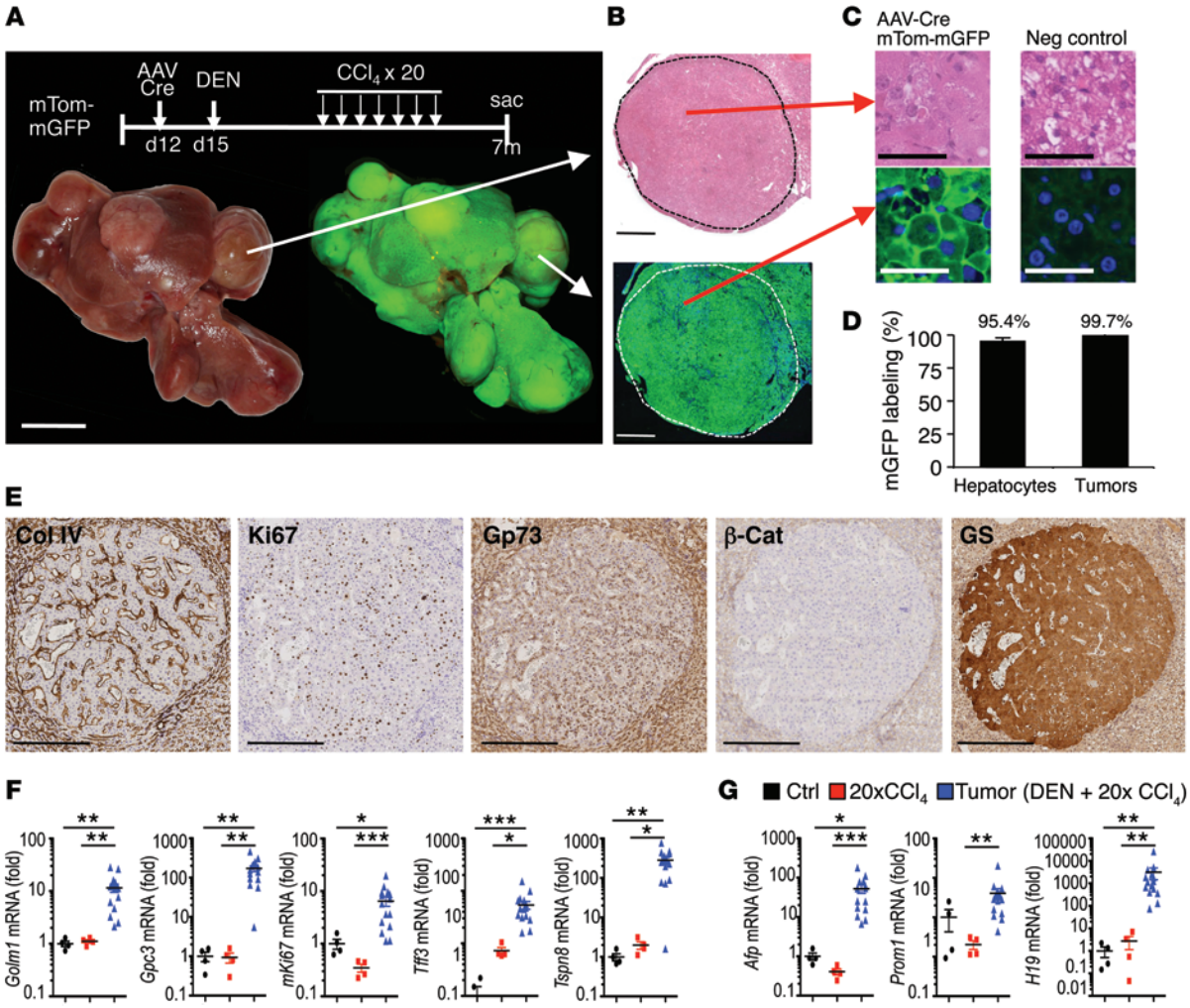

Figure 3. Genotoxic HCC derives from hepatocytes. mTom-mGFP Cre reporter mice (n = 10) were infected with AAV8-*Tbg-Cre* to selectively label hepatocytes, followed by treatment with DEN and 20 injections of CCl_4 for HCC induction. (**A**–**C**) Representative images and fluorescent images of livers from DEN+CCl_4-treated mice (**A**) and H&E- and GFP-stained liver sections at low (**B**) and high (**C**) magnification, including an mTom-mGFP negative control. (**D**) Quantification of GFP-labeled hepatocytes and tumors (average of all mice, n = 10). (**E**) Typical HCC features were confirmed by collagen IV staining, increased Ki67 and glutamine synthetase levels, and altered Gp73 and β-catenin (β-Cat) staining. (**F** and **G**) HCC markers (**F**) and progenitor markers (**G**) were determined by qPCR. Scale bars: 1 cm (**A**); 1 mm (**B**); 50 μm (**C**); 300 μm (**E**). $^*P < 0.05$, $^{**}P < 0.01$, $^{***}P < 0.01$ by Kruskal-Wallis and Dunn's post-hoc test.

tumors in DEN+CDE and DEN+DDC experiments were a result of incomplete hepatocyte labeling rather than being LPC/biliary compartment derived. Similar to the DEN+CCl_4 model, DEN+CDE- and DEN+DDC-induced tumors showed high expression of HCC markers and progenitor and hepatoblast markers (Supplemental Figure 7, E and F, and Table 2).

HCC originates from hepatocytes in nongenotoxic HCC models. To exclude the possibility that our observations on hepatocyte origin were specific to the models used or caused by preferential metabolism of carcinogens in hepatocytes, we additionally tested the cellular origin in DEN-free HCC models. For this purpose, we first investigated *Mdr2*^{KO} mice, which spontaneously develop inflammation, fibrosis, and HCC, thus reproducing the sequence of events that lead to the majority of human HCCs (43). In the *Mdr2*^{KO} model, AAV8-*Tbg-Cre*–mediated hepatocyte labeling via the ZsGreen Cre reporter exceeded 95.7%, without labeling desmin-positive HSCs, F4/80-positive Kupffer cells, cytokeratin-positive cholangiocytes, or endomucin-positive endothelial cells (Supplemental Figure 8A). As this model not only lacks the confounding effects of hepatocellular DEN metabolism but also incorporates an abundance of progenitor/hepatoblast markers in the injured liver (Figure 4H), it provides an ideal setting for determining in an unbiased manner the cell population from which HCCs originate in the chronically injured, inflamed, and fibrotic liver. All HCCs from *Mdr2*^{KO} mice (n = 9 mice, 25 of 25 tumors) arose from AAV8-*Tbg-Cre*–labeled hepatocytes with macroscopic and microscopic ZsGreen tumor fluorescence (Figure 4, A–D, and Table 2) and colocalization of ZsGreen with HNF4α within tumors (Figure 4E). Tumors from *Mdr2*^{KO} mice were typical HCCs, with altered collagen IV expression, high expression of the proliferation marker Ki67, and upregulation of the tumor markers *Golm1*, *Tff3*, and *Tspn8* mRNA (Figure 4, F–H), as determined by IHC and qPCR. The few ZsGreen-negative cells within tumors were endomucin-positive endothelial cells and F4/80-positive Kupffer

Table 2. Hepatocyte tracing in HCC models

Mouse	HCC induction	Liver analyzed (*n*)	Livers with HCCs (%)	Number of HCCs analyzed per liver (min–max)	Total no. of HCCs analyzed	% of HCCs traced as having hepatocyte origin	% of K9$^+$ HCCs (no. of pos. HCCs/ no. of analyzed tumors)	% of A6$^+$ HCCs (no. of pos. HCCs/ no. of analyzed tumors)
lox-stop-lox mTom-mGFP Cre reporter mice plus AAV8-*Opn-CreERT2*	DEN+CCl_4	10	100%	1–35	186	99.5% (185/186)	17.1% (19/111 analyzed)	36.9% (41/111 analyzed)
lox-stop-lox mTom-mGFP Cre reporter mice plus AAV8-*Opn-CreERT2*	DEN+CDE	4	100%	19–41	118	98.3% (116/118)	14.5% (12/83 analyzed)	56.6% (47/83 analyzed)
lox-stop-lox mTom-mGFP Cre reporter mice plus AAV8-*Opn-CreERT2*	DEN+DDC	3	100%	5–22	46	95.7% (44/46)	11.4% (4/35 analyzed)	40.0% (14/35 analyzed)
Mdr2^{KO} - ZsGreen Cre reporter mice plus AAV8-*Tbg-Cre*	*Mdr2*^{KO}	9	100%	1–6	25	100% (25/25)	38.9% (7/18 analyzed)	66.7% (12/18 analyzed)
Pten$^{fl/fl}$ - mTom-mGFP Cre reporter mice	*Pten* deletion (AAV8-*Tbg-Cre*)	8	100%	2–4	12	100% (123/123)	Not det.	Not det.
Pten$^{fl/fl}$ - mTom-mGFP Cre reporter mice	*Pten* deletion (AAV8-*Tbg-Cre*)	4	100%	15–44	123	100% (123/123)	Not det.	Not det.

cells (Supplemental Figure 8B). To further confirm these findings in another nongenotoxic model, we determined whether hepatocyte-specific deletion of *Pten* triggers HCC. *PTEN* is a tumor-suppressor gene that shows reduced expression in approximately 50% of human HCC cases and an inverse correlation with survival (44) and whose deletion by albumin-*Cre* — which deletes *PTEN* in both the hepatocyte and LPC/biliary compartment (Supplemental Figure 9) — triggers HCC development in mice (45). To provide evidence for hepatocytes as the cellular source of HCC in a genetic model, we either deleted *Pten* specifically in hepatocytes via AAV8-*Tbg-Cre* or in the LPC/biliary compartment via tamoxifen-inducible *K19-CreERT* (39). AAV8-*Tbg-Cre*–induced hepatocyte-specific deletion of *Pten* resulted in the development of tumors with HCC features including increased expression of glypican 3, Ki67, pancytokeratin, and phosphorylated-AKT (p-AKT) (Supplemental Figure 10CCl_4, A and B, and Table 2), and tumors were derived from hepatocytes, as demonstrated by green fluorescence (Supplemental Figure 10, C and D). By contrast, K19-driven *Pten* deletion resulted in an expansion of the cytokeratin-positive biliary compartment but never led to HCC development (Supplemental Figure 10, E and F). These data again demonstrate that the LPC/biliary compartment is not endowed with the capacity to form HCCs in mice. Finally, we also subjected *Opn-Cre* mice to chronic treatment with a CDE-deficient diet as a complementary LPC/biliary compartment–labeling approach. This model was accompanied by a florid DR. HCCs were less common than in other models but were YFP negative and hence not of LPC origin (Supplemental Figure 10, G and H, and Table 1). Together, these data provide multiple lines of evidence that hepatocytes, and not the LPC/biliary compartment, are the cellular source for HCC in nongenotoxic tumor models.

HSCs do not represent a cellular source for HCC. Recent studies have suggested HSCs as an alternative source of LPCs and hepatocytes (20). However, this concept remains controversial and is not supported by fate tracing in mice (46). To determine whether HSC-derived LPCs or hepatocytes might be the source for HCC, HSCs were labeled by *Lrat-Cre* in combination with ZsGreen or TdTomato mice, a system that efficiently and selectively tags HSCs in the liver (46). In line with our previous studies in multiple injury models (46), we did not detect a significant number of HSC-derived hepatocytes in mice that underwent injury-driven hepatocarcinogenesis induced by DEN+CCl_4 (data not shown). Moreover, we did not find any tumors that were derived from *Lrat-Cre*–labeled cells (Figure 5, A–C), with all fluorescent cells within tumors being desmin positive (Figure 5D) and HNF4α and cytokeratin negative (Supplemental Figure 11A). Similar observations were made in the *Mdr2*^{KO} model, in which no tumor cell was derived from *Lrat-Cre*–labeled HSCs (Figure 5, E, F, H, and Supplemental Figure 11B). In both models, tumors revealed typical HCC characteristics such as altered collagen IV and Gp73 expression patterns and increased Ki67 staining (Figure 5, C and G). While most tumors contained moderate numbers of *Lrat-Cre*–labeled cells, some tumors in both the DEN+CCl_4 and *Mdr2*^{KO} models displayed stronger accumulation of *Lrat-Cre*–labeled, desmin-positive HSCs (Supplemental Figure 11, C and D). However, even in the few tumors that showed strong Cre reporter fluorescence, fluorescent cells colocalized with desmin, without any overlap of the *Lrat-Cre*–induced Cre reporter TdTomato with either HNF4α or cytokeratin (Supplemental Figure 11, E and F). These findings are consistent with our data on the exclusive contribution of hepatocytes to HCC formation in the DEN+CCl_4 and the *Mdr2*^{KO} models and further exclude the possibility that HCCs originate from HSC-derived hepatocytes.

Progenitor cells within HCCs originate from hepatocytes. Consistent with our data showing high mRNA expression of the progenitor/hepatoblast markers *Afp*, *Prom1*, and *H19* in tumors (Figure 2E, Supplemental Figure 3C, and Supplemental Figure 7F), we observed abundant A6- and AFP-positive cells, and to a lesser extent cytokeratin 19–positive (K19-positive) cells, within HCC

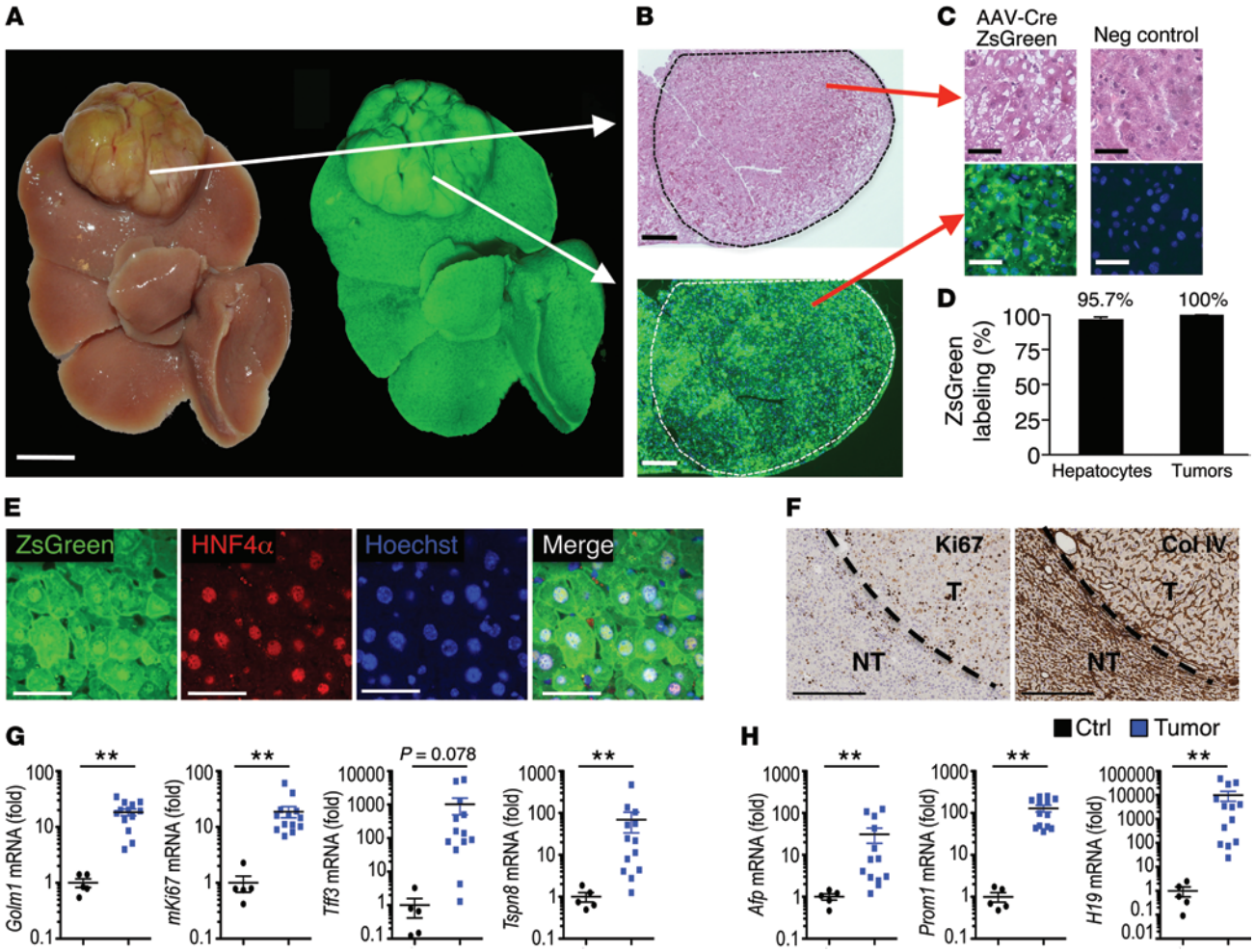

Figure 4. HCCs derive from hepatocytes in the *Mdr2*^{KO} HCC model. *Mdr2*^{KO} mice expressing the ZsGreen Cre reporter (n = 9) were infected with AAV8-*Tbg-Cre* to selectively label hepatocytes and sacrificed at 12 to 14 months of age. (**A**–**C**) Representative images and fluorescent images of whole livers from *Mdr2*^{KO} mice (**A**) as well as H&E- and Hoechst-stained frozen liver sections at low (**B**) and high (**C**) power, including a ZsGreen negative control. (**D**) Quantification of GFP-labeled hepatocytes and tumors (average of all mice). (**E**) Costaining demonstrated that HNF4α-positive tumor cells were ZsGreen positive. (**F**) Typical HCC features were confirmed by increased Ki67 expression and altered collagen IV staining. (**G** and **H**) HCC markers (**G**) and progenitor markers (**H**) were determined by qPCR (n = 5 control livers and n = 14 tumors). Scale bars: 1 cm (**A**); 300 μm (**B**); 50 μm (**C** and **E**); 500 μm (**F**). $^{**}P < 0.01$ by Mann-Whitney U test.

nodules in all DEN-based models (Figure 1D, Figure 6, A–C, E, F, Supplemental Figure 12, Supplemental Figure 13, A and B, and Supplemental Figure 14, A and B). Instead of interpreting these markers as a sign of LPC origin, we investigated the alternative hypothesis that AFP-, A6-, and K19-positive cells within HCCs may be hepatocyte-derived cells that underwent dedifferentiation. Confocal microscopy demonstrated that in AAV8-*Tbg-Cre* mice, virtually all A6-positive cells within DEN+CCl_4-, DEN+DDC-, and DEN+CDE-induced tumors also coexpressed mGFP (Figure 6A, Supplemental Figure 12, Supplemental Figure 13B, and Supplemental Figure 14B), thus demonstrating their hepatocytic origin. These data were confirmed by AFP and K19 staining, which showed that AFP-positive cells (Figure 6C, Supplemental Figure 12, Supplemental Figure 13A, and Supplemental Figure 14A) and K19-positive cells (Figure 6B and Supplemental Figure 12) within tumors were mGFP positive and therefore hepatocyte derived. In contrast, there were almost no A6-positive cells that coexpressed mGFP outside of the tumors (Figure 6, A and D, Supplemental Figure 12, Supplemental Figure 13B, and Supplemental Figure 14B). Moreover, only a small amount of K19-positive cells outside the tumor areas were mGFP positive (Figure 6, B and D). Similar findings were made in the *Mdr2*^{KO} model, in which most K19-positive and A6-positive cells within tumors, but not in the surrounding liver, were hepatocyte derived (Supplemental Figure 15, A and B). Consistent with these findings, we observed in *Opn-CreERT2* mice that A6-positive cells within tumors were YFP negative, whereas the A6-positive DR surrounding the tumors was YFP positive (Figure 6, E and H). K19 staining confirmed that YFP-positive cells outside the tumors expressed K19, while K19-positive cells within the HCCs were YFP negative (Figure 6, F and H, and Supplemental Figure 2, C and D). AFP-positive cells were only found within the tumors and were YFP negative (Figure 6G). Together, these data suggest that A6-, K19-, and AFP-positive cells within tumors are hepatocyte derived, but that most A6- and K19-positive cells outside the tumors (AFP-positive cells were extremely rare outside the tumors; Figure 6D) were derived from the LPC/biliary compartment.

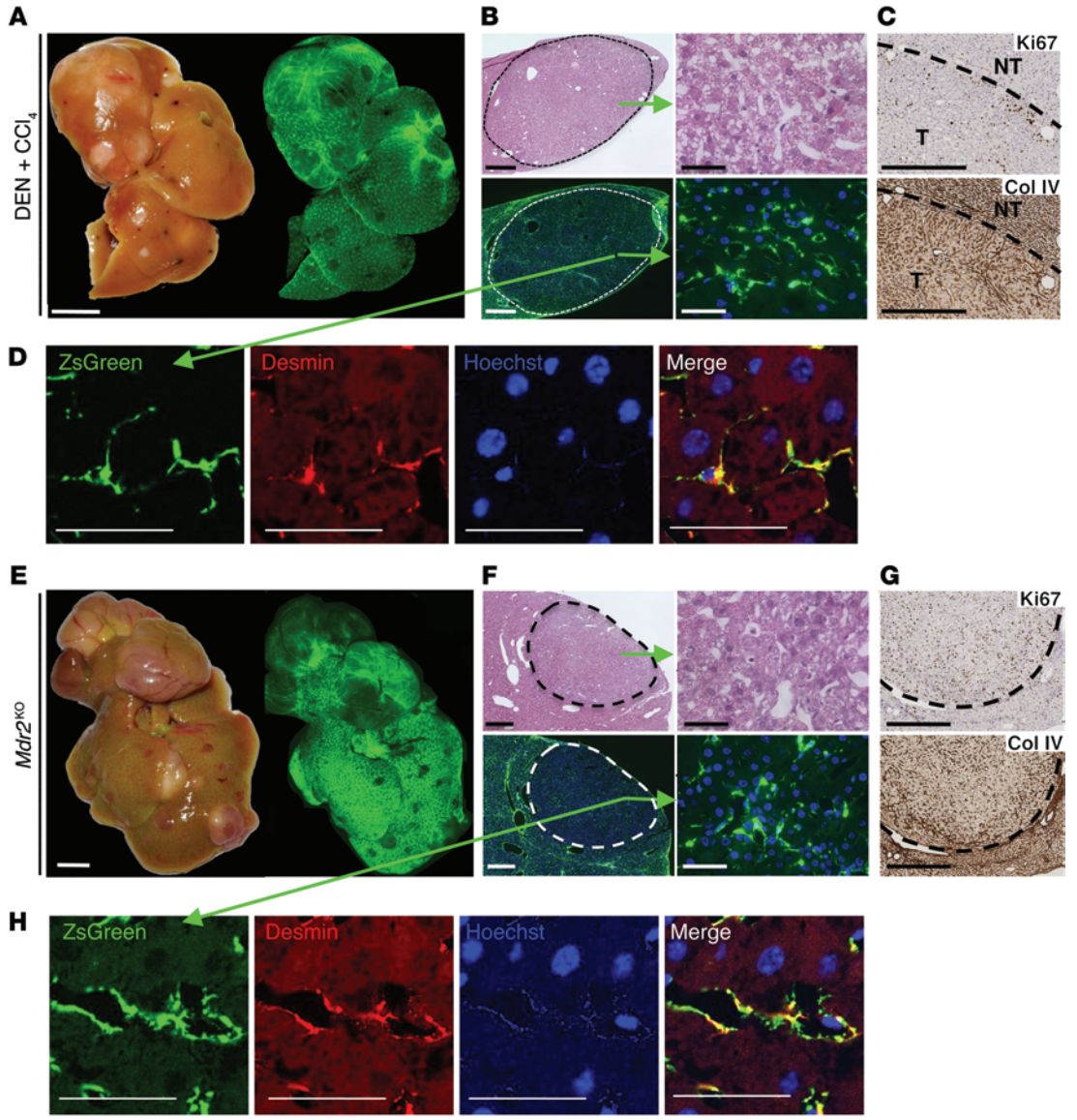

Figure 5. HCCs are not derived from HSCs. (**A**–**D**) *Lrat-Cre* Tg mice expressing the ZsGreen Cre reporter (n = 4) were treated with DEN and 20 injections of CCl_4 for HCC induction. Representative images and fluorescent images of livers from DEN+CCl_4-treated mice (**A**) as well as H&E- and Hoechst-stained frozen liver sections at low and high magnification show green fluorescent HSCs but no green fluorescent tumor cells derived from HSCs (**B**). Typical HCC features were confirmed by collagen IV staining and increased Ki67 expression (**C**). ZsGreen-positive cells colocalized with the HSC marker desmin (**D**). (**E**–**H**) *Mdr2*^{KO} mice expressing *Lrat-Cre* and the ZsGreen Cre reporter (n = 8) were sacrificed at 12 months of age. Representative images and fluorescent images of whole livers (**E**) as well as H&E- and Hoechst-stained frozen liver sections at low and high magnification show green fluorescent HSCs but no green fluorescent tumor cells derived from HSCs (**F**). Typical HCC features were confirmed by increased Ki67 expression and altered collagen IV staining (**G**). ZsGreen-positive cells colocalized with the HSC marker desmin (**H**). Scale bars: 5 mm (**A** and **E**); 500 μm (**B**, left panel and **F**, left panel); 50 μm (**B**, right panel and **F**, right panel); 500 μm (**C** and **G**); 50 μm (**D** and **H**).

Discussion

Despite its nomenclature, the cellular source of HCC remains elusive. Hepatocytes are not only the target of oncogenic hepatotrophic viruses and most hepatotoxins, but also have a stem cell–like capacity for nearly infinite regeneration (47), making them a primary candidate for the cellular source of HCC. However, the LPC/biliary compartment has the capacity to differentiate into hepatocytes (10, 13, 19), and LPCs are commonly found in dysplastic lesions and HCCs (30, 31, 48), suggesting that the LPC/biliary compartment could be an alternative source for subsets of HCCs, in particular those with a progenitor signature. In support of this, both cell populations have been demonstrated to have the ability to induce HCC when transduced with a combination of H-RAS and SV40LT (32). Despite their known capacity to differentiate into HCCs after forced expression of oncogenes, the relative contribution of these cell types to HCC formation in endogenous HCC models, which occur in the setting of chronic injury and inflammation, remains unknown. Our fate-tracing data support the hypothesis that hepatocytes constitute the main cellular source of HCC in mice and that the LPC/biliary compartment does not function as a source of HCC in mice. Our analysis not only includes several models in which HCCs expressed an

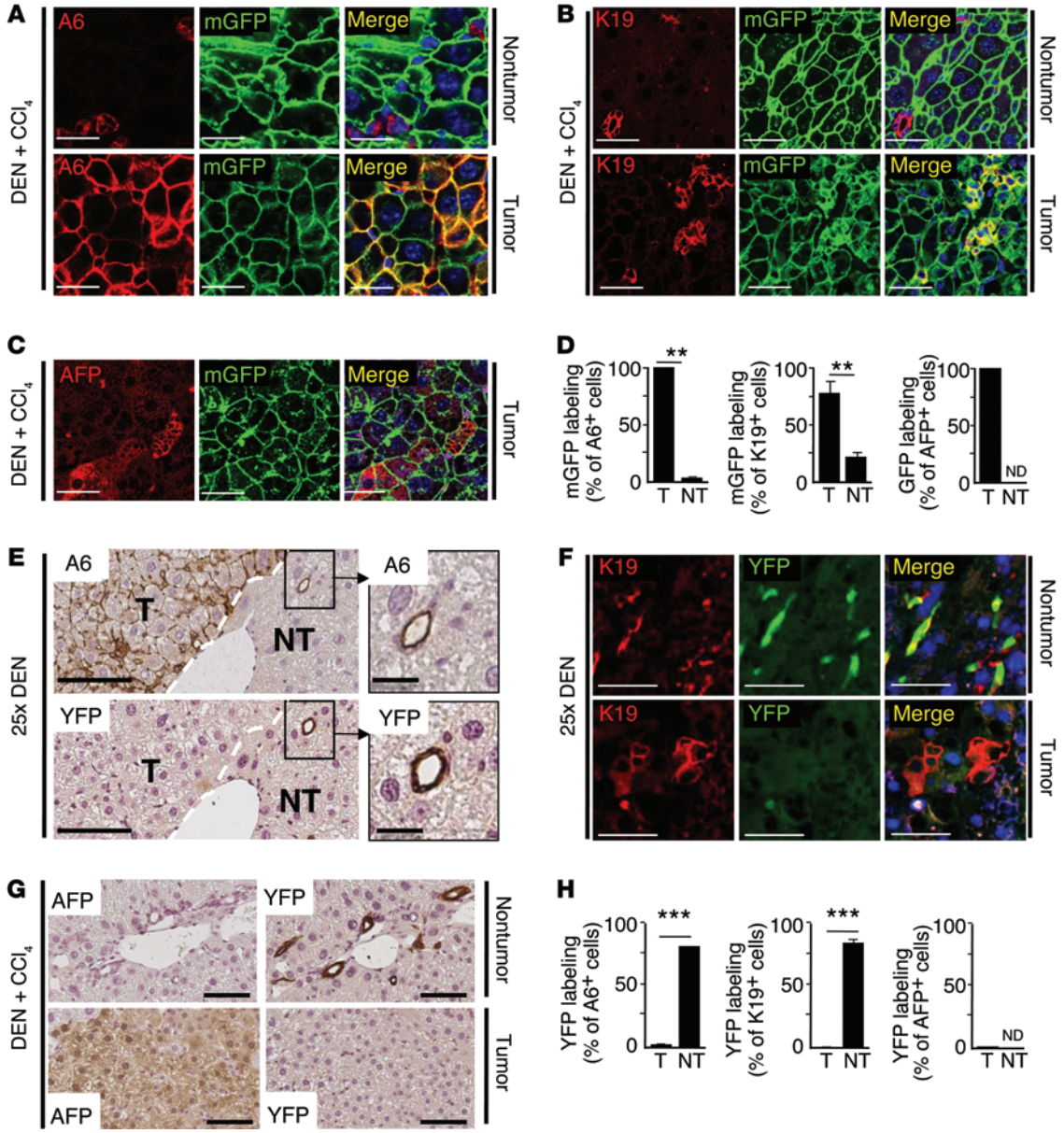

Figure 6. A6-, K19-, and AFP-positive liver progenitors within HCCs are derived from hepatocytes. (**A**–**D**) To determine the cellular origin of liver progenitor cells within HCCs, colocalization of the progenitor markers A6 (**A**), K19 (**B**), and AFP (**C**) with mGFP was determined by confocal microcopy in tumor and nontumor areas of mTom-mGFP mice whose hepatocytes had been labeled via AAV8-*Tbg-Cre* and that were subsequently treated with DEN and CCl_4. Quantification of mGFP of A6-, K19-, and AFP-positive cells in tumor and nontumor areas (n = 10 each) (**D**). (**E**–**H**) Colocalization of the progenitor/hepatoblast markers A6 (**E**, serial sections), K19 (**F**, fluorescence), and AFP (**G**, serial sections) with YFP in tumor and nontumor areas of *Opn-CreERT2* mice treated with 25 injections of DEN or with DEN+CCl_4. Quantification of YFP with A6-, K19-, or AFP-positive cells (**H**) in tumor or nontumor areas. $^{**}P < 0.01$, $^{***}P < 0.001$ by 2-sided Student's t test. ND, nondetectable. Scale bars: 50 μm (**A**–**C** and insert in **E**); 100 μm (**E**–**G**).

abundance of progenitor/hepatoblast markers, but also carcinogen-free models in which HCC formation could be assessed without the possibly confounding preferential metabolization of carcinogens by hepatocytes. Consistent with our data showing that 99.4% and 100% of HCCs in the DEN+CCl_4 and *Mdr2*^{KO} models, respectively, were hepatocyte derived, we never observed HCCs originating from the LPC/biliary compartment. Because of the early age at which mice were injected, our hepatocyte labeling did not reach the levels that were seen in adult mice in previous studies (14, 40). As we did not label all hepatocytes but nonetheless observed only a single GFP-negative tumor in a total of 186 tumors and none in the *Mdr2*^{KO} model, we conclude that this tumor most likely arose from unlabeled hepatocytes. Moreover, we did not find any evidence that HSCs, a recently suggested alternative source for liver progenitors and hepatocytes (20), are a cellular source of HCC. Our findings are consistent with those of recent studies showing either a dominant or exclusive role of hepatocytes in hepatocyte repopulation, even in settings in which LPCs expanded and were considered a key source of newly generated hepatocytes (14–18). Likewise, our finding that murine HCCs

are not derived from HSCs is consistent with our previous finding that HSCs do not contribute to the hepatocyte or progenitor pool in multiple chronic injury mouse models (46). In agreement with the data presented here, a recent study using *Hnf1b-CreERT* labeling of the LPC/biliary compartment found no contribution of this compartment to HCC in DEN- or *Mdr2*^{KO}-induced HCC (49), which complements the findings presented here. However, in contrast to our study, the authors did not positively identify the cellular source of HCC.

Our data demonstrate a fundamental difference between the liver and organs such as the intestine, skin, and hematopoetic system, in which cancer is thought to be derived from stem cells (21–25). This is consistent with the key role of the terminally differentiated hepatocyte in generating new hepatocytes in the normal and injured liver (8, 14, 16–18). In view of the recently suggested hypothesis that the number of stem cell doublings determines cancer risk across various organs (50), the hepatocyte should be seen as a fully differentiated cell with stem cell–like functions that is at risk for malignant transformation with increasing numbers of doublings, similar to other stem cell populations. This hypothesis is compatible with the high rate of cancer observed in patients with chronic liver disease and constant hepatocyte turnover (51).

Recent studies found that hepatocytes have a high degree of plasticity and dedifferentiate into immature progenitors or biliary-type cells in response to specific signals (40, 41). These data are consistent with our finding that hepatocyte-derived tumor cells express progenitor/biliary markers, suggesting a similar ability of hepatocyte-derived tumor cells to dedifferentiate into progenitor-like cells. It is likely that such a dedifferentiation allows cells to adapt to specific challenges in the environment and presents an advantage for the tumor. Accordingly, tumors with a progenitor signature have worse prognosis (31).

Our study contains several limitations. Although we have confirmed hepatocyte origin and excluded LPC/biliary and HSC origins for a number of HCC models including various genotoxic and genetic models, we cannot fully exclude the possibility that progenitors have the ability to generate tumors in other settings. As a wide range of infectious, metabolic, genetic, and toxic liver diseases can result in HCC development in patients, studies in additional hepatocarcinogenesis models — possibly using humanized mice to mimic HCC arising in the setting of hepatitis B virus–induced (HBV-induced) and HCV-induced hepatitis — are required to broaden the findings presented here. Also, recent fate-tracing studies in zebrafish have suggested that when hepatocyte proliferation is completely blocked — which so far has not been achieved in murine injury models — regeneration occurs to a significant degree from the biliary compartment (19). However, a catastrophic event with complete hepatocyte failure is characteristic of acute liver failure but not of HCC, in which injury is typically mild and chronic, similar to that in the animal models used. Our study mimicked several key features that are characteristic of human hepatocarcinogenesis such as chronic liver injury, fibrosis, and alterations in PTEN expression, but could not address possible intrinsic differences between mouse and human hepatocytes or progenitor cells. As such, the contribution of the DR to functional hepatocytes in humans remains a matter of debate (48), and therefore it cannot be excluded that the DR is a cellular source of HCC in patients. Future studies need to address the cellular origin of human HCC, e.g., through the use of humanized mice for fate tracing and/or by showing that human hepatocytes have the same plasticity as mouse hepatocytes and are able to dedifferentiate into LPCs.

Methods

Tracing of liver progenitor cells in hepatocarcinogenesis. To track LPCs and biliary cells, we used the previously described *Opn-CreERT2* mice (15). The Tg mice were on a CD1-enriched background, and males were used in all experiments. To achieve *Cre-LoxP* recombination, tamoxifen (T5648; Sigma-Aldrich) dissolved in corn oil at a concentration of 30 mg/ml was injected i.p. at 100 mg/kg BW on day 21 pp unless otherwise specified. In all experiments, Tg mice without tamoxifen injection ($n \geq 5$) were used in parallel as a negative control for Cre recombination. Mice had free access to water and food at all times. To determine the contribution of LPCs to HCC, tamoxifen administered i.p. on day 21 pp was followed by i.p. injections of DEN (35 mg/kg BW) for 25 weeks starting at 6 weeks of age ($n = 44$) (36). At the start of chronic DEN treatment and up to the end of the experiment, 1 group of mice was fed a standard rodent chow diet ($n = 22$), while another group ($n = 22$) was placed on a high-fat diet (HFD) consisting of 60% saturated fat (D12492; Research Diets). Because the effect of an HFD was to hasten tumor development, with no alteration in the nature of the tumors, data are presented for the entire group. In a second model, a single i.p. injection of DEN (6 mg/kg BW) (N0258; Sigma-Aldrich) was given on day 15 pp, and tamoxifen was administered i.p. either on days 9–10 pp ($n = 16$) or on days 21–22 pp ($n = 25$), and mice were sacrificed at 18 and 9 months of age, respectively. In a third experiment, mice were injected with tamoxifen on days 9–10 pp, followed by a single i.p. injection of DEN (6 mg/kg BW) on day 15 pp and 20 weekly injections of CCl_4 (0.5 μl/g BW). Mice were sacrificed 2–4 weeks after the last CCl_4 dose ($n = 6$). Other tamoxifen-injected (day 21 pp) *Opn-CreERT2* mice ($n = 12$) were treated with a CDE diet for 50 weeks starting at 8 weeks of age. Mice were sacrificed at 58 weeks of age or earlier, when the general status of the mice was altered (BW loss, decreased activity, or prostration). The DEN+CCl_4 model was additionally used in *K19-CreERT* mice (39) ($n = 5$) coexpressing the mTom-mGFP Cre reporter; these mice received tamoxifen (80 μg/g i.p.) on day 10 pp and DEN on day 15 pp, followed by 25 weekly injections of CCl_4.

Tracing of hepatocytes in hepatocarcinogenesis. To genetically label hepatocytes, lox-stop-lox mTom-mGFP Cre reporter mice (52) were infected with AAV8-*Tbg-Cre*, resulting in mGFP expression in AAV8-*Tbg-Cre*–infected hepatocytes and in those of their offspring. For this purpose, mice were injected i.v. with 1×10^{11} genome copies of AAV8-*Tbg-Cre* (53) on day 12 pp. To induce HCC, AAV8-*Tbg-Cre*–infected mice received a single i.p. dose of DEN (25 mg/kg BW) (Sigma-Aldrich) on day 15 pp. Subsequently, hepatic carcinogenesis was promoted by chronic injury using 3 different models. Four weeks after receiving DEN, some mice were treated with a total of 15 weekly injections of CCl_4 (0.5 μl/g i.p., dissolved in oil at a ratio of 1:3, given once per week, $n = 10$) as described previously (38). For hepatocyte tracing in mice receiving DEN+CCl_4, only mice with at least 90% hepatocyte labeling in nontumor sections were analyzed. Some mice were fed a DDC diet ($n = 3$) for 6 weeks starting 4 weeks after receiving DEN. Some mice were fed a CDE diet for 6 weeks starting 4 weeks after the DEN injection ($n = 4$).

Mdr2-KO–mediated hepatocarcinogenesis. To genetically label hepatocytes in the *Mdr2*^{KO} model, lox-stop-lox ZsGreen Cre reporter mice (54) were infected with AAV8-*Tbg-Cre*, resulting in ZsGreen expression in AAV8-*Tbg-Cre*–infected hepatocytes and in those of their offspring. *Mdr2*^{KO} mice (on an FVB background) that had been bred with ZsGreen Cre reporter mice (on a C57Bl/6 background) and backcrossed once with *Mdr2*^{KO} mice (n = 9) were injected i.v. with 1 × 10^{11} genome copies of AAV8-*Tbg-Cre* (53) on day 14 pp. *Mdr2*^{KO} mice received additionally up to 25 weekly injections of CCl_4 in order to accelerate hepatocarcinogenesis. Mice were sacrificed at 12 to 14 months of age following screening for HCC by ultrasound.

PTEN-mediated hepatocarcinogenesis studies. As a nongenotoxic model of HCC, *Pten*$^{WT/WT}$ (n = 4) or *Pten*$^{fl/fl}$ mice (n = 8), some of which were additionally carrying the mTom-mGFP Cre reporter, were injected with AAV8-*Tbg-Cre* (1 × 10^{11} genome copies i.v.) at 7 weeks of age, resulting in hepatocyte-specific deletion of *Pten*. To delete *Pten* specifically in the progenitor/ductular compartment, *Krt19-CreERT* mice (39) were crossed with *Pten*$^{WT/WT}$ (n = 4) or *Pten*$^{fl/fl}$ mice (n = 4) and injected with tamoxifen (100 μg/ i.p.) at 2 weeks of age.

Lrat-Cre–mediated HSC labeling. To determine whether HSCs might be a cellular source for HCC, *Lrat-Cre* mice coexpressing ZsGreen or TdTomato Cre reporters (54) were injected i.p. with DEN (25 mg/kg BW) on day 15 pp, followed by 20 weekly injections of CCl_4 (n = 4). Mice were sacrificed 2 weeks after the last CCl_4 injection. *Mdr2*^{KO} mice coexpressing *Lrat-Cre* and ZsGreen or TdTomato (n = 8) served as a second HCC model. Mice were sacrificed at 12 to 14 months of age following HCC screening by ultrasound.

Immunohistochemical and immunofluorescence analysis. Following sacrifice and rapid excision of the liver, tumor and nontumor tissues were macroscopically identified and either fixed in 4% formalin for histological examination or snap-frozen in liquid nitrogen for gene expression analysis.

For histological analysis, 4-μm formalin-fixed, paraffin-embedded liver sections and frozen liver sections were analyzed. For immunohistochemical analysis, slides were incubated for 1 hour at 37°C with primary Abs against YFP (catalog Ab6673; Abcam); cytokeratin 19 (Developmental Studies Hybridoma Bank, University of Iowa); HNF4α (catalog PP-H1415 from R&D Systems or catalog sc-6556 from Santa Cruz Biotechnology Inc.); AFP (catalog 14550-1-AP; Proteintech); OPN (catalog AF808; R&D Systems); α–smooth muscle actin (α-SMA) (MyBioSource); Ki67 (Tec3; Dako); desmin (catalog RB-9014-P; Lab Vision); pancytokeratin (catalog Z0622; Dako); CD31 (catalog 14-0311-81; eBioscience); progenitor marker A6 (55) (a gift of Valentina Factor, NIH, Bethesda, Maryland, USA) or F4/80 (catalog MCA497A64; AbD Serotec); collagen IV (catalog CL50451 AP-1; Cedarlane); Ki67 (rabbit monoclonal; Thermo Scientific); Gp73 (catalog sc-48001; Santa Cruz Biotechnology Inc.); or glutamine synthetase (catalog ab16802; Abcam). Detection was performed using either fluorescent secondary Abs with various fluorescent conjugates: anti-rabbit (donkey anti-rabbit, A21207; chicken anti-rat A21472; or chicken anti-goat A21468; all used at 1:200; all from Invitrogen), or with HRP-conjugated secondary Abs (anti-rat Ig-HRP, E0468; anti-goat Ig-HRP P0449; anti-mouse Envision K4001; or anti-rabbit Envision K4003; used at 1:50 to 1:200; all from Dako), with subsequent DAB exposure and hematoxylin counterstaining. For DAB staining, serial sections were used. Fluorescent images were taken on a Nikon A1 confocal laser microscope (Nikon Instruments) using a ×20 standard lens or ×40 and ×60 oil-immersion lenses or an Axiovert 200 fluorescence microscope (Carl Zeiss). For some images and for quantification, 4–6 sections were merged. Nonfluorescent images were taken with a Zeiss microscope coupled with an AxioCam camera (MR3; Carl Zeiss). Omission of the first Ab with an otherwise identical procedure or a sample lacking specific protein expression served as a negative control.

Quantification of hepatocyte and tumor labeling. Labeling efficiency in the biliary/progenitor compartment was determined as previously reported (15). Briefly, K19-YFP double-positive cells relative to the total number of K19-positive cells in 25 random nontumor fields of view per section per mouse were quantified and expressed as a percentage. Timing for tamoxifen injection (days 9–21) or DEN treatment on day 15 did not modify the labeling efficiency. The percentage of A6-YFP and AFP-YFP double-positive cells was quantified using the same methodology.

For macroscopic imaging and determination of the percentage of GFP-labeled tumors, livers were visualized under a Leica MZ 16F fluorescence dissecting microscope. The ratio between green tumors and all tumors in each mouse was determined and expressed as a percentage. To quantify the GFP labeling for hepatocytes, frozen sections from nontumor tissue were used. Labeling efficiency was evaluated by quantification of GFP-positive hepatocytes relative to the total number of GFP-positive and mTomato-positive hepatocytes and expressed as a percentage.

The percentage of K19-GFP double-positive cells was determined by quantification of K19-GFP double-positive cells relative to the total K19-positive cell numbers in tumor and nontumor areas in DEN+CCl_4-, DEN+CDE-, and DEN+DDC-treated mice groups. The percentage of A6-GFP double-positive cells was determined by the same approach.

RNA isolation and qPCR. RNA was isolated from cells and liver tissue by column purification and on-column DNAse treatment. After reverse transcription, mRNA levels were determined by qPCR on an Applied Biosystem 7300 Real-Time PCR cycler, using Applied Biosystems TaqMan primers and probes for *Afp*, *Prom1*, *H19*, *mKi67*, *Golm1*, *Tspan8*, *Tff3*, and *Gpc3*. All qPCRs were quantified using relative standard curves and normalized to 18S expression. mRNA levels in *Opn-Cre* samples were determined using SYBR green and results expressed as fold induction relative to control untreated liver using the ΔΔCt method.

Determination of hepatocytic and nonparenchymal cell markers in AAV8-Tbg-Cre–labeled liver cells. To determine which hepatic cell types were labeled by AAV8-*Tbg-Cre*, ZsGreen Cre reporter mice were infected with AAV8-*Tbg-Cre*. One week later, mice were sacrificed. Following perfusion with collagenase, green fluorescent cells were sorted by FACS from the entire liver cell suspension. After RNA isolation and reverse transcription, qPCR was used to measure hepatocyte markers (*Alb*, *Ttr*), cholangiocyte markers (*Krt7*, *Krt19*), HSC markers (*Des*, *Lrat*), endothelial cell markers (*Pecam*, *Vwf*), and macrophage markers (*Emr1*, *Cd68*). To determine the percentage of these markers in the isolated green fluorescent cell fraction, cDNA from pure reference populations of primary cholangiocytes, HSCs, endothelial cells, and hepatic macrophages (46) was used.

Comparative genomic hybridization and syntenic analysis. Custom-designed 8x60K arrays (AMADID 41078; Agilent Technologies) were used for aCGH. Nineteen different formalin-fixed and paraffin-embedded HCC nodules and 2 unaffected liver tissues were microdissected, and genomic DNA was extracted using a DNAeasy

FFPE kit (QIAGEN), as previously described (56). Genomic DNA (125 ng) from test and control DNA was labeled with Cy3-dUTP and Cy5-dUTP, respectively, using the Enzo Life Sciences CGH-labeling protocol. Purification of labeled nucleotides, hybridization, scanning, and data extraction were performed according to the manufacturer's instructions and as described previously (57). On the basis of H&E microscopic assessments, 50% of the estimated proportion of tumor cells were used for the CGH call function (56, 57). Human syntenic regions were queried using an in-house compiled R function and the BioMart database (www.biomart.com). Ward's method and Euclidean distance were used to hierarchically cluster and visualize the copy number profiles, again using the in-house–written R function. The aCGH set described in ref. 42 was downloaded from the NCBI's Gene Expression Omnibus database (GEO GSE8351) and analyzed as described previously (57).

Statistics. Statistical analysis was performed using Prism software (GraphPad Software). Differences between 2 groups were calculated using a 2-sided Student's *t* test or the Mann-Whitney *U* test. Significance of differences between multiple groups was determined by the Kruskal-Wallis test, followed by Dunn's post-hoc test. A *P* value of less than 0.05 was considered statistically significant. All data are expressed as the mean ± SD.

Study approval. All animal experiments were performed with the approval of the Université catholique de Louvain Animal Welfare Committee (2012/UCL/MD/026) and the IACUC of Columbia University (protocols AC-AM6851 and AC-AAAE6450), in accordance with European Union regulations and NIH guidelines for the care and use of laboratory animals, respectively.

Acknowledgments

This work is supported by grants from the NIH (R01CA190844 and U54CA163111, to R.F. Schwabe); the Fund for Scientific Medical Research (FRS-FNRS, Belgium, to I.A. Leclercq); the Fondation contre le Cancer (PDR T.1067.14-P and C/2014/207, to I.A. Leclercq); the Belgian Federal Science Policy Office (Interuniversity Attraction Poles program, network P7/83-HEPRO2, to I.A. Leclercq and F.P. Lemaigre); and by a European Research Council (ERC) Starting Grant and a grant for Biomedizinische Forschung from the Peter-Hans Hofschneider Stiftung (both to M. Heikenwälder). X. Mu was supported by a grant from the China Scholarship Council. I.A. Leclercq is an FRS-FNRS research associate.

Address correspondence to: Robert F. Schwabe, 1150 St. Nicholas Ave., Russ Berrie Pavilion, Room 412C, New York, New York 10032, USA. Phone: 212.851.5462; E-mail: rfs2102@cumc.columbia.edu. Or to: Isabelle Leclercq, Avenue Mounier 53, B1.52.01, tour Vesale +2, 1200 Brussels, Belgium. Phone: 32.2764.5273; E-mail: isabelle.leclercq@uclouvain.be.

1. Parkin DM, Bray F, Ferlay J, Pisani P. Estimating the world cancer burden: Globocan 2000. *Int J Cancer*. 2001;94(2):153–156.
2. Forner A, Llovet JM, Bruix J. Hepatocellular carcinoma. *Lancet*. 2012;379(9822):1245–1255.
3. Miyajima A, Tanaka M, Itoh T. Stem/progenitor cells in liver development, homeostasis, regeneration, and reprogramming. *Cell Stem Cell*. 2014;14(5):561–574.
4. Donati G, Watt FM. Stem cell heterogeneity and plasticity in epithelia. *Cell Stem Cell*. 2015;16(5):465–476.
5. Clevers H. The intestinal crypt, a prototype stem cell compartment. *Cell*. 2013;154(2):274–284.
6. Blanpain C, Fuchs E. Epidermal stem cells of the skin. *Annu Rev Cell Dev Biol*. 2006;22:339–373.
7. Zaret KS, Grompe M. Generation and regeneration of cells of the liver and pancreas. *Science*. 2008;322(5907):1490–1494.
8. Friedman JR, Kaestner KH. On the origin of the liver. *J Clin Invest*. 2011;121(12):4630–4633.
9. Wilson JW, Leduc EH. Role of cholangioles in restoration of the liver of the mouse after dietary injury. *J Pathol Bacteriol*. 1958;76(2):441–449.
10. Wang X, Foster M, Al-Dhalimy M, Lagasse E, Finegold M, Grompe M. The origin and liver repopulating capacity of murine oval cells. *Proc Natl Acad Sci U S A*. 2003;100(suppl 1):11881–11888.
11. Boulter L, Lu WY, Forbes SJ. Differentiation of progenitors in the liver: a matter of local choice. *J Clin Invest*. 2013;123(5):1867–1873.
12. Duncan AW, Dorrell C, Grompe M. Stem cells and liver regeneration. *Gastroenterology*. 2009;137(2):466–481.
13. Huch M, et al. Long-term culture of genome-stable bipotent stem cells from adult human liver. *Cell*. 2015;160(1–2):299–312.
14. Malato Y, et al. Fate tracing of mature hepatocytes in mouse liver homeostasis and regeneration. *J Clin Invest*. 2011;121(12):4850–4860.
15. Espanol-Suner R, et al. Liver progenitor cells yield functional hepatocytes in response to chronic liver injury in mice. *Gastroenterology*. 2012;143(6):1564–1575.
16. Yanger K, et al. Adult hepatocytes are generated by self-duplication rather than stem cell differentiation. *Cell Stem Cell*. 2014;15(3):340–349.
17. Tarlow BD, et al. Bipotential adult liver progenitors are derived from chronically injured mature hepatocytes. *Cell Stem Cell*. 2014;15(5):605–618.
18. Schaub JR, Malato Y, Gormond C, Willenbring H. Evidence against a stem cell origin of new hepatocytes in a common mouse model of chronic liver injury. *Cell Rep*. 2014;8(4):933–939.
19. He J, Lu H, Zou Q, Luo L. Regeneration of liver after extreme hepatocyte loss occurs mainly via biliary transdifferentiation in zebrafish. *Gastroenterology*. 2014;146(3):789–800.
20. Kordes C, Sawitza I, Gotze S, Herebian D, Haussinger D. Hepatic stellate cells contribute to progenitor cells and liver regeneration. *J Clin Invest*. 2014;124(12):5503–5515.
21. Barker N, et al. Crypt stem cells as the cells-of-origin of intestinal cancer. *Nature*. 2009;457(7229):608–611.
22. Zhu L, et al. Prominin 1 marks intestinal stem cells that are susceptible to neoplastic transformation. *Nature*. 2009;457(7229):603–607.
23. Youssef KK, et al. Identification of the cell lineage at the origin of basal cell carcinoma. *Nat Cell Biol*. 2010;12(3):299–305.
24. Lapouge G, et al. Identifying the cellular origin of squamous skin tumors. *Proc Natl Acad Sci U S A*. 2011;108(18):7431–7436.
25. Shlush LI, et al. Identification of pre-leukaemic haematopoietic stem cells in acute leukaemia. *Nature*. 2014;506(7488):328–333.
26. Sell S. Is there a liver stem cell? *Cancer Res*. 1990;50(13):3811–3815.
27. Sigal SH, Brill S, Fiorino AS, Reid LM. The liver as a stem cell and lineage system. *Am J Physiol*. 1992;263(2 pt 1):G139–G148.
28. Roskams T. Liver stem cells and their implication in hepatocellular and cholangiocarcinoma. *Oncogene*. 2006;25(27):3818–3822.
29. Andersen JB, et al. Progenitor-derived hepatocellular carcinoma model in the rat. *Hepatology*. 2010;51(4):1401–1409.
30. Roskams TA, Libbrecht L, Desmet VJ. Progenitor cells in diseased human liver. *Semin Liver Dis*. 2003;23(4):385–396.
31. Lee JS, et al. A novel prognostic subtype of human hepatocellular carcinoma derived from hepatic progenitor cells. *Nat Med*. 2006;12(4):410–416.
32. Holczbauer A, et al. Modeling pathogenesis of primary liver cancer in lineage-specific mouse cell types. *Gastroenterology*. 2013;145(1):221–231.
33. Guest RV, et al. Cell lineage tracing reveals a biliary origin of intrahepatic cholangiocarcinoma. *Cancer Res*. 2014;74(4):1005–1010.
34. Fan B, et al. Cholangiocarcinomas can originate from hepatocytes in mice. *J Clin Invest*. 2012;122(8):2911–2915.
35. Sekiya S, Suzuki A. Intrahepatic cholangiocarcinoma can arise from Notch-mediated conversion of hepatocytes. *J Clin Invest*. 2012;122(11):3914–3918.
36. Heindryckx F, et al. Kinetics of angiogenic changes in a new mouse model for hepatocellular carcinoma. *Mol Cancer*. 2010;9:219.
37. Veronesi U, Boyle P, Goldhirsch A, Orecchia R, Viale G. Breast cancer. *Lancet*.

2005;365(9472):1727–1741.
38. Dapito DH, et al. Promotion of hepatocellular carcinoma by the intestinal microbiota and TLR4. *Cancer Cell*. 2012;21(4):504–516.
39. Means AL, Xu Y, Zhao A, Ray KC, Gu G. A CK19(CreERT) knockin mouse line allows for conditional DNA recombination in epithelial cells in multiple endodermal organs. *Genesis*. 2008;46(6):318–323.
40. Yanger K, et al. Robust cellular reprogramming occurs spontaneously during liver regeneration. *Genes Dev*. 2013;27(7):719–724.
41. Yimlamai D, et al. Hippo pathway activity influences liver cell fate. *Cell*. 2014;157(6):1324–1338.
42. Schlaeger C, et al. Etiology-dependent molecular mechanisms in human hepatocarcinogenesis. *Hepatology*. 2008;47(2):511–520.
43. Trauner M, Fickert P, Wagner M. MDR3 (ABCB4) defects: a paradigm for the genetics of adult cholestatic syndromes. *Semin Liver Dis*. 2007;27(1):77–98.
44. Hu TH, et al. Expression and prognostic role of tumor suppressor gene PTEN/MMAC1/TEP1 in hepatocellular carcinoma. *Cancer*. 2003;97(8):1929–1940.
45. Horie Y, et al. Hepatocyte-specific Pten deficiency results in steatohepatitis and hepatocellular carcinomas. *J Clin Invest*. 2004;113(12):1774–1783.
46. Mederacke I, et al. Fate tracing reveals hepatic stellate cells as dominant contributors to liver fibrosis independent of its aetiology. *Nat Commun*. 2013;4:2823.
47. Overturf K, al-Dhalimy M, Ou CN, Finegold M, Grompe M. Serial transplantation reveals the stem-cell-like regenerative potential of adult mouse hepatocytes. *Am J Pathol*. 1997;151(5):1273–1280.
48. Fausto N. Liver regeneration and repair: hepatocytes, progenitor cells, and stem cells. *Hepatology*. 2004;39(6):1477–1487.
49. Jors S, et al. Lineage fate of ductular reactions in liver injury carcinogenesis. *J Clin Invest*. 2015;125(6):2445–2457.
50. Tomasetti C, Vogelstein B. Cancer etiology. Variation in cancer risk among tissues can be explained by the number of stem cell divisions. *Science*. 2015;347(6217):78–81.
51. Luedde T, Kaplowitz N, Schwabe RF. Cell death and cell death responses in liver disease: mechanisms and clinical relevance. *Gastroenterology*. 2014;147(4):765–783.
52. Muzumdar MD, Tasic B, Miyamichi K, Li L, Luo L. A global double-fluorescent Cre reporter mouse. *Genesis*. 2007;45(9):593–605.
53. Miller RA, et al. Adiponectin suppresses gluconeogenic gene expression in mouse hepatocytes independent of LKB1-AMPK signaling. *J Clin Invest*. 2011;121(6):2518–2528.
54. Madisen L, et al. A robust and high-throughput Cre reporting and characterization system for the whole mouse brain. *Nat Neurosci*. 2010;13(1):133–140.
55. Engelhardt NV, Factor VM, Medvinsky AL, Baranov VN, Lazareva MN, Poltoranina VS. Common antigen of oval and biliary epithelial cells (A6) is a differentiation marker of epithelial and erythroid cell lineages in early development of the mouse. *Differentiation*. 1993;55(1):19–26.
56. Vucur M, et al. RIP3 inhibits inflammatory hepatocarcinogenesis but promotes cholestasis by controlling caspase-8- and JNK-dependent compensatory cell proliferation. *Cell Rep*. 2013;4(4):776–790.
57. Haybaeck J, et al. A lymphotoxin-driven pathway to hepatocellular carcinoma. *Cancer Cell*. 2009;16(4):295–308.